ACS APPLIED MATERIALS & INTERFACES

Research Article

www.acsami.org

Fabrication of Noble-Metal Catalysts with a Desired Surface Wettability and Their Applications in Deciphering Multiphase Reactions

Demeng Wang,[†] Shun Wang,*[,†] Huile Jin,[†] Weiming Zhang,[†] Yun Yang,[†] Aiping Sun,[†] Tiandi Tang,[†] and Jichang Wang*[,†,‡]

[†]Nano-materials and Chemistry Key Laboratory, Wenzhou University, Wenzhou, Zhejiang 325027, People's Republic of China

[‡]Department of Chemistry and Biochemistry, University of Windsor, Windsor, Ontario, Canada N9B 3P4

ABSTRACT: Noble-metal Pd and Pt catalysts with a wide range of surface wettability were fabricated through an electrochemical approach and were characterized with scanning electron microscopy, energy-dispersive X-ray spectroscopy, transmission electron microscopy, and atomic force microscopy. The importance of surface wettability of solid catalysts in multiphase reactions—especially their correlation to the nature of the studied chemical system—was investigated by reducing oxygen in an alkaline solution and oxidizing hydrogen peroxide and sodium formate in alkaline or buffered solutions at the as-prepared catalysts. These experiments illustrate that the nature of a multiphase reaction plays a critical role in determining the influence of surface wettability on the catalyst performance, providing a unique approach to decipher the reaction process. The investigation allows us to gain new insights into the electrochemical oxidation of sodium formate.

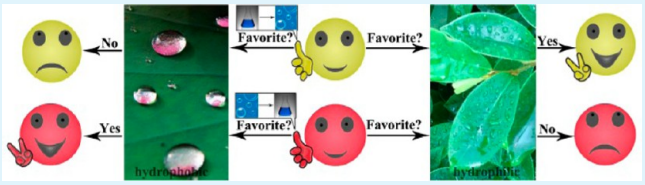

KEYWORDS: *surface wettability, electrocatalysis, noble metals, multiphase reactions*

1. INTRODUCTION

Multiphase reactions play an extremely important role in the modern society, ranging from petroleum refining to specialty chemicals to environment protection.[1−11] A fine example is hydrogen fuel cells, in which hydrogen and oxygen gases are oxidized and reduced at solid anode and cathode catalysts, respectively, resulting in the production of liquid water. Catalysis at the electrode surface is no doubt essential in the above processes. Developing new catalysts as well as improving the performance of existing catalysts has attracted a great deal of attention in the last three decades. Parameters such as the size,[3−8] shape,[9−11] architecture,[12] and exposed facets[13−17] of the catalyst have been explored in achieving efficient catalysis. Hybrids or doped noble-metal catalysts have also been developed to improve both the catalytic efficiency and antifouling properties.[18−25] The use of nanostructured materials significantly increases the effective surface area and the number of active sites; however, surface properties such as wettability may be altered concomitantly.[26] Notably, influences of surface wettability on catalytic performance have been observed in several systems, in which hydrophilic−hydrophobic balance drives the competitive adsorption of reactants and products.[27,28]

In contrast to the great awareness of the importance of surface wettability in catalysis,[29−33] correlations among the wettability, catalytic efficacy, and the nature of multiphase reactions have not received much deserved attention, especially their potential applications in elucidating the mechanism of a multiphase reaction. In general, the wettability of a solid catalyst can be manipulated either at the molecular level with low-surface-energy coatings such as fluorinated compounds or at macroscopic levels with rough surfaces. Herein, we reported a simple way of fabricating solid palladium and platinum catalysts with a wide range of surface wettability and, more importantly, demonstrated how the influence of wettability on the efficiency of a solid catalyst was correlated to the nature of the studied multiphase reactions. Specifically, our experiments showed that, depending on whether a gas-phase reagent is a reactant or a product, the catalyst wettability might have opposite effects on the catalysis (see Scheme 1 for illustration). Such a correlation provides a new route to gain insights into the mechanisms of multiphase reactions. The selected model catalysts (palladium and platinum) represent two catalysts that have found wide applications in the chemical industry.[34]

2. EXPERIMENTAL SECTION

Analytical-grade $PdCl_2$ (>99%), $H_2PtCl_6{\cdot}6H_2O$, sodium formate (HCOONa), hydrogen peroxide (H_2O_2, 30% w/w), KOH, Na_2HPO_4, and NaH_2PO_4 were purchased from Sigma−Aldrich and were used as received. H_2SO_4 (>98%) was obtained from Aladdin. Phosphate buffer solution (0.1 M, pH 7.0) was prepared by mixing standard solutions of Na_2HPO_4 and NaH_2PO_4. H_2O_2 solution was prepared everyday. All aqueous solutions were prepared with ultrapure water obtained from a Milli-Q Plus system (18.2 MΩ, Millipore, Bedford, MA, USA).

Received: February 24, 2013
Accepted: April 11, 2013
Published: April 11, 2013

Scheme 1. Illustration of the Correlation of Surface Wettability, Catalysis, and the Nature of Multiphase Reactions

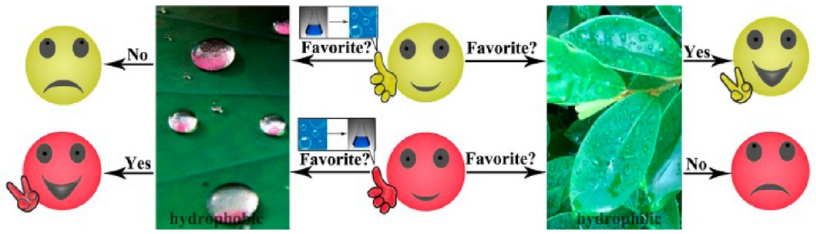

All electrochemical experiments were conducted with a CHI 760d electrochemical workstation (Chenhua, Shanghai, PRC) at 25 ± 1 °C. A conventional three-electrode cell was used, in which the tin-doped indium oxide (ITO) glass, purchased from Nanbo Co. Ltd. (Shenzhen, PRC), served as the working electrode. A platinum sheet and a saturated calomel electrode (SCE) were used as a counter electrode and reference electrode, respectively. The ITO glass (1.0 cm × 1.8 cm) was cleaned sequentially by sonicating for 10 min each time in acetone, ethanol, and distilled water. Only a 1.0 cm^2 area of the ITO was exposed to the 0.1 M H_2SO_4 electrolyte solution containing 0.02 M $PdCl_2$ or 0.05 M H_2PtCl_6 for the production of corresponding catalysts. The applied potential was −0.5 V (vs SCE) for reducing palladium salt and was changed to −0.3 V (vs SCE) for reducing platinum salt. After electrodeposition, the ITO samples were thoroughly rinsed with deionized water and were dried at 50 °C in a vacuum oven.

Field-emission scanning electron microscopy (FE-SEM) and energy-dispersive spectroscopy (EDX) of the catalyst deposit were taken on a Nova NanoSEM 200 scanning electron microscope (FEI, Inc.). The average roughness of these deposit layers was determined in air by a Nanoscope IIIa atomic force microscope (DI Instruments, USA) in a tapping mode, using Nanoprobe cantilevers/Si_3N_4 integral tips with a spring constant of 20−100 N m^{-1}. Transmission electron microscopy (TEM) was performed on a Hitachi Model H-800 TEM microscope, in which the TEM specimen was prepared by mechanically scratching the palladium or platinum deposits using dissecting forceps in the presence of a small drop of ethanol. Static water contact angle (CA) of the catalyst layer was measured using a SL200B instrument (Solon Tech, Shanghai, China). The CA value was fitted by the Young−Laplace equation. Throughout this research, the CA was measured at five different spots and the average value was reported.

Cyclic voltammetry (CV) of hydrogen peroxide was carried out in a 0.1 M phosphate buffer solution (pH 7.0) that was bubbled with N_2 for 20 min prior to the experiment. A nitrogen atmosphere was maintained throughout the measurements. The linear sweep voltammetry (LSV) of oxygen reduction was carried out in an O_2-saturated 0.1 M KOH solution. The voltammetric experiments of sodium formate were performed in 0.1 M KOH solution containing 0.04 M HCOONa, purged with N_2 for 20 min before starting the experiment. The scan rate was 50 mV s^{-1} in all CV measurements. The effective surface areas (ESAs) of the palladium and platinum layers were determined with a CV technique,[12,35] where the scan took place in a 0.1 M KOH solution. Integration of the charge consumed during the formation of the surface oxide enabled the estimation of the ESA of the catalyst layer using a reported value of 430 μC cm^{-2} for palladium. ESA of the platinum films was calculated using the method and parameters reported in the literature.[35]

3. RESULTS AND DISCUSSION

Figure 1 presents SEM images of the palladium catalysts that were electrochemically fabricated with different deposition times: 200 s (Figure 1a), 300 s (Figure 1b), 400 s (Figure 1c), and 500 s (Figure 1d). Figure 1a indicates that the ITO substrate was fully covered by palladium particles that were a mixture of concave cubes and tetrahedrons. The inset in Figure 1a illustrates that this surface is hydrophilic, with a measured

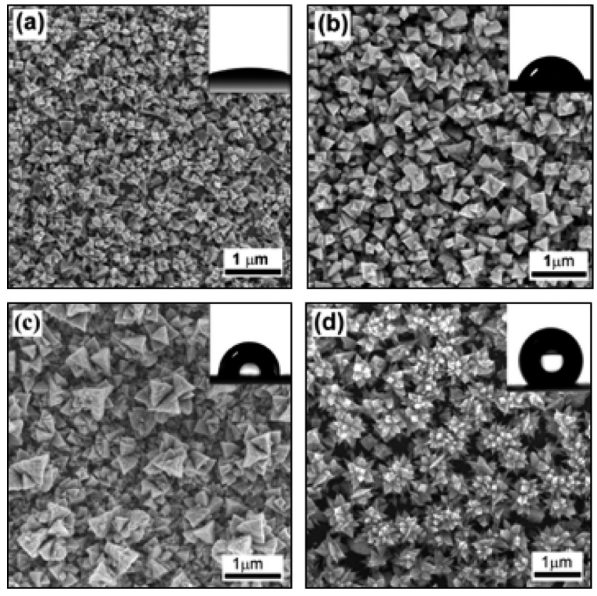

Figure 1. SEM images of the palladium deposits prepared with different deposition times: (a) 200 s, (b) 300 s, (c) 400 s, and (d) 500 s. The insets are the measurement of the static water contact angle (CA) at the Pd deposits.

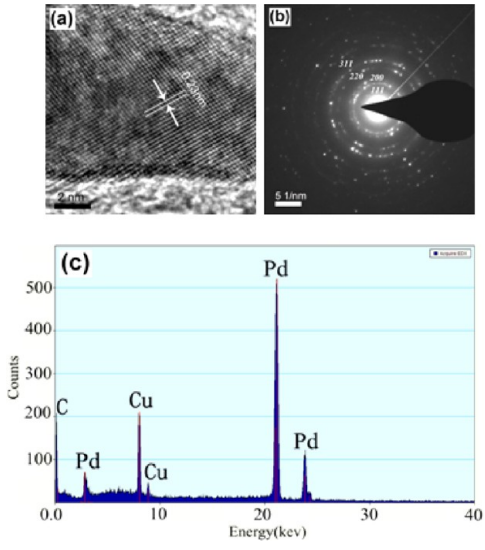

Figure 2. (a) High-resolution transmission electron microscopy (HRTEM) image, (b) selected-area electron diffraction (SAED), and (c) energy-dispersive X-ray spectroscopy (EDX) spectrum of the palladium deposits shown in Figure 1a.

CA value of 15.0° ± 0.9°. Since the ITO surface is fully covered by palladium particles, the observed surface properties shall arise from these assembled palladium particles rather than from

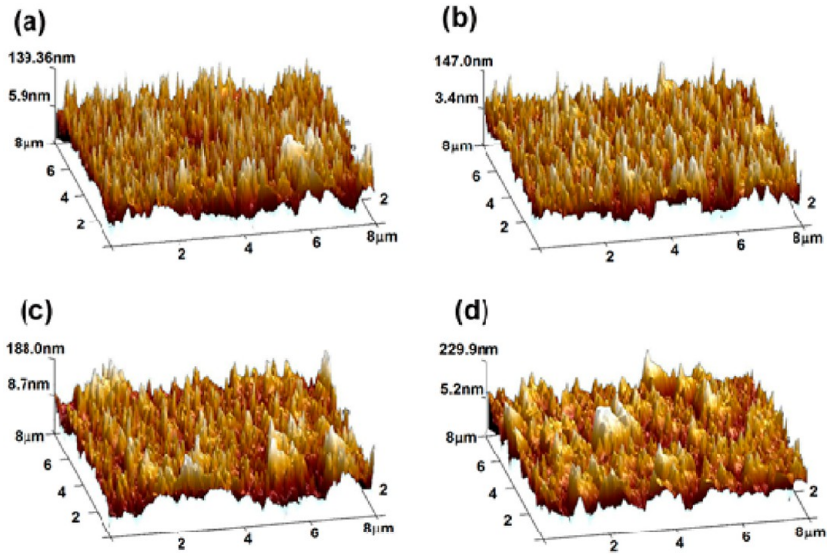

Figure 3. Atomic force microscopy (AFM) images of the palladium deposits with CA values of (a) 15.0° ± 0.9°, (b) 53.0° ± 0.8°, (c) 84.0° ± 0.5°, and (d) 125.0° ± 0.4°.

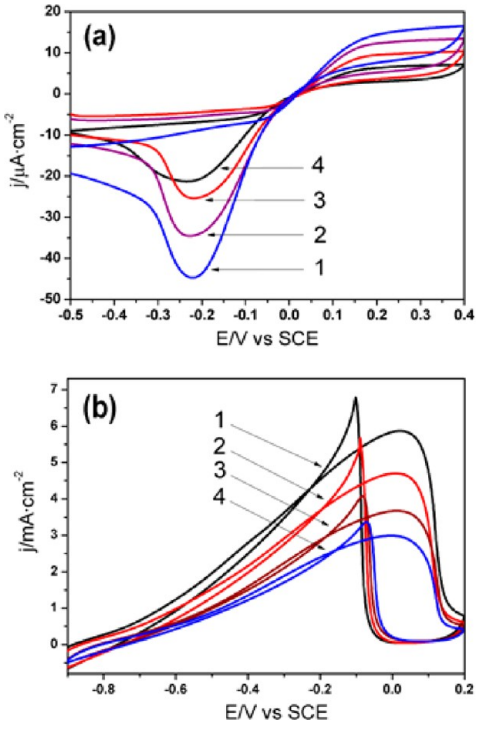

Figure 4. Cyclic voltammograms of (a) 0.01 M H_2O_2 in 0.1 M phosphate buffer solution, and (b) 0.01 M sodium formate in 0.1 M KOH solution at the Pd electrodes that have different CAs: (1) 15.0° ± 0.9°, (2) 53.0° ± 0.8°, (3) 84.0° ± 0.5°, and (4) 125.0° ± 0.4°. The scan rate was 50.0 mV s^{-1}.

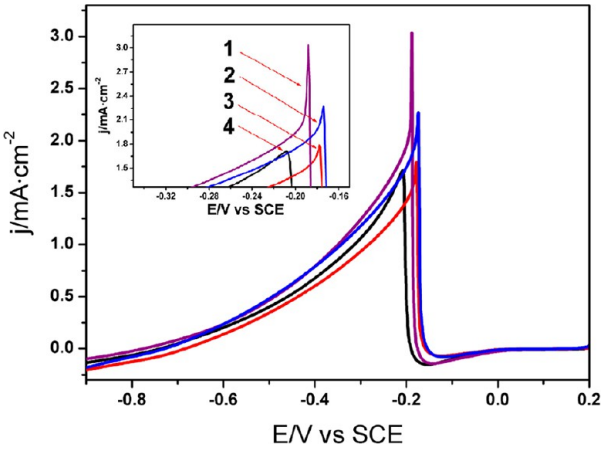

Figure 5. Linear sweep voltammogram of formate in a 0.1 M KOH solution at palladium electrodes with different CAs: (1) 15.0° ± 0.9°, (2) 53.0° ± 0.8°, (3) 84.0° ± 0.5°, and (4) 125.0° ± 0.4°. Here, the palladium electrodes were first scanned in a 0.1 KOH solution from −0.8 V to 0.2 V. Other conditions are the same as those used in Figure 4b.

the ITO substrate. This conclusion is further supported by directly measuring the surface wettability of ITO substrates, which has an average CA of 66.8° ± 0.8°. As the deposition time was increased to 300 s in Figure 1b, these palladium particles grew bigger and became dominated by tetrahedrons. The growth of these tetrahedrons seems to be uniform. Measurements of the CA yielded a value of 53.0° ± 0.8°, indicating that the surface wettability decreased.

Employing a longer deposition time led to greater change in the particle size, where almost one-third of the nanoparticles grew significantly larger (see Figure 1c). The inset in Figure 1c shows that the CA has increased to 84.0° ± 0.5°, i.e., turning into a hydrophobic surface as a result of prolonging the deposition time. When the deposition period was increased to 500 s in Figure 1d, flower-like particles were achieved, in which the individual flower was larger than the particle obtained in Figure 1c. The petals of these flowers are similar in size to the particles seen in Figure 1a. The palladium catalyst layer in Figure 1d has a CA of 125.0° ± 0.4°, which is close to being a superhydrophobic surface.

The above-prepared Pd catalysts were further characterized by high-resolution transmission electron microscopy (HRTEM), selected-area electron diffraction (SAED), and (c) energy-dispersive X-ray spectroscopy (EDX) in Figures 2a, 2b, and 2c, respectively. The HRTEM image in Figure 2a illustrates that the fringes are separated by 2.3 Å, which agrees with the

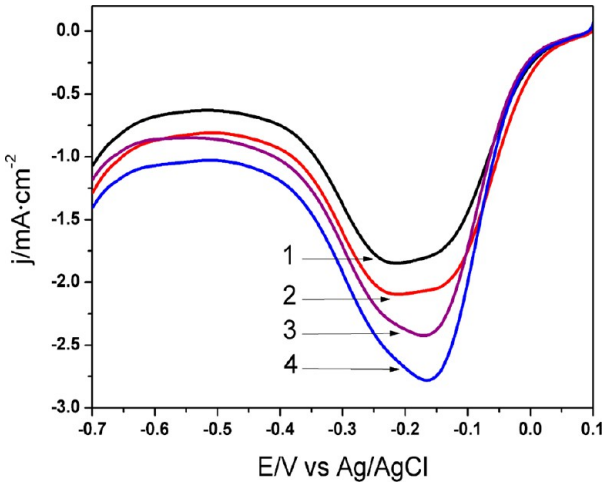

Figure 6. Linear sweep voltammogram of oxygen reduction in 0.1 M KOH solution at the Pd electrodes having different CAs: (1) 15.0° ± 0.9°, (2) 53.0° ± 0.8°, (3) 84.0° ± 0.5°, and (4) 125.0° ± 0.4°. The scan rate was 50.0 mV s^{-1}.

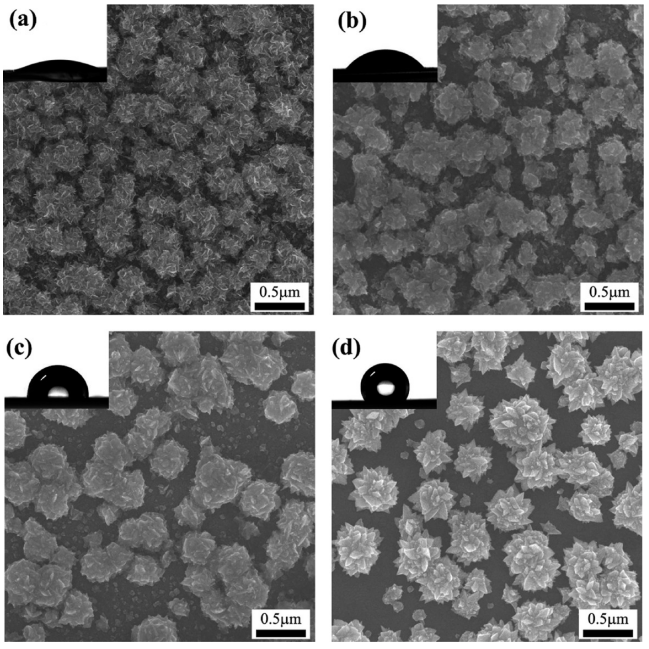

Figure 7. SEM images of the platinum deposits prepared with different deposition times: (a) 200 s, (b) 250 s, (c) 300 s, and (d) 350 s. The insets show the static water contact angle (CA).

{1 1 1} lattice spacing of face-centered cubic (fcc) metallic palladium (International Centre for Diffraction Data (ICDD) File Card No. 05-0681). The SAED analysis in Figure 2b demonstrates that these palladium nanoparticles are polycrystalline. The EDX spectrum in Figure 2c confirmed that those particles consisted of elemental palladium only; the Cu and C peaks arise from the substrate used to prepare the specimen.

In order to understand the variation of CA, the surface roughness of the above Pd deposits was measured with atomic force microscopy (AFM) in a tapping mode. As presented in Figure 3, the AFM measurements show that the average roughness of the above palladium deposits are 32.2 ± 1.3 nm (Figure 3a), 39.0 ± 0.5 nm (Figure 3b), 47.0 ± 1.3 nm (Figure 3c), and 0.4 ± 0.6 nm (Figure 3d). This indicates that the transition from a hydrophilic surface to a near-superhydrophobic surface is related to the increase of the surface roughness, which is a result of changes in the sizes and shapes of these individual palladium particles.

Figure 4a presents cyclic voltammograms of H_2O_2 in a 0.10 M phosphate buffer solution. According to the literature,[36,37] electro-oxidation of H_2O_2 produces oxygen molecules. Because the charge transfer process is slow, the cyclic voltammograms of H_2O_2 do not have a well-developed anodic peak. However, it is clear that the palladium catalyst layer with CA = 15.0° produced the highest current density. Overall, the current density decreased with the increase of the CA, i.e., a hydrophilic palladium surface favored the electro-oxidation of H_2O_2. Existing mechanisms have suggested that the above electrochemical reaction processes involve the reversible binding of H_2O_2 to electrochemically generated Pd(II) surface sites, reduction of the site, and the competitive adsorption of H^+ and O_2. A hydrophilic surface would facilitate the escape of oxygen molecules that have been produced at the active sites, which concomitantly makes the active site available for the binding of H_2O_2.[36,37] As a result, catalysts with a hydrophilic surface have better performance in catalysis. On the reverse scan, an isolated reduction peak was achieved, which corresponded to the reduction of Pd(II). Since this process involved the direct reduction of Pd(II) on the electrode surface, the magnitude of this reduction peak was determined by the amounts of Pd(II) produced during the forward scan and therefore exhibited similar dependence on the wettability of the palladium catalyst layer.

In Figure 4b, electrochemical oxidations of sodium formate were investigated. It has been proposed that the electrolysis of formate in alkaline solution resulted in the formation of hydrogen atoms (H) at the anode.[38−40] A hydrophilic surface facilitates the escape of hydrogen molecules (H_2) to free the active sites on the electrode surface; therefore, the oxidation peak of formate should grow as the wettability of the catalyst layer increases, which is indeed the case seen in Figure 4b. On the reverse scan, however, there is also an oxidation peak. Such a peak has been frequently attributed to the fouling of the catalyst by intermediates produced during the forward scan.[39,40] Similar fouling behaviors are well-documented in electrochemical reactions such as in fuel cells in which electrooxidation of simple alcohols produces intermediates that adsorb on the catalysts. A fingerprint of the fouling behavior is the occurrence of a large oxidation, rather than a reduction peak on the reverse scan. If the anodic peak on the reverse scan in Figure 4b is indeed due to the oxidation of the intermediate product (atomic hydrogen, H), the palladium layer with a more hydrophilic surface would produce a lower anodic peak, because of its poor retention of H_2 molecules. This rationale is contrary to the experimental results observed in Figure 4b, where the highest anodic peak on the reverse scan also belongs to the palladium catalyst that has the highest hydrophilic surface.

To shed light on the above discrepancy, in Figure 5, we first oxidized Pd electrodes in a NaOH solution and then added sodium formate to the NaOH solution to perform a negative linear scan from 0.2 V to −0.8 V (vs SCE). The waveform of the achieved anodic peak in Figure 5 largely resembles the peaks observed in Figure 4b. The start potential of the oxidation peak is almost identical to that in Figure 4b as well. Since there is no oxidation of formate prior the anodic peak, the oxidation peak observed in Figure 5, as well as on the reverse

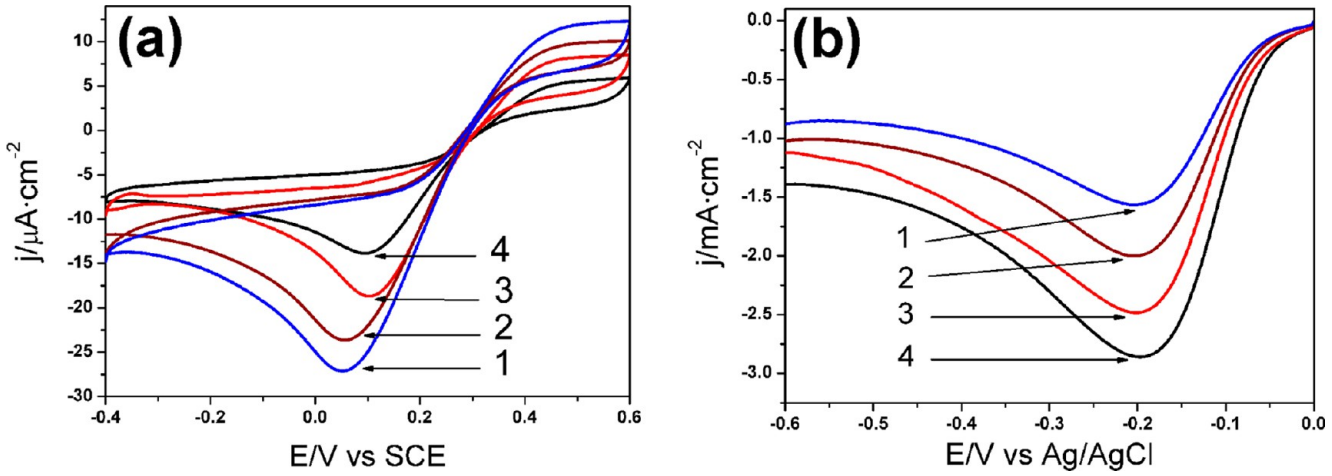

Figure 8. (a) Cyclic voltammograms of 0.01 M H_2O_2 in 0.1 M phosphate buffer solution, and (b) linear sweep voltammograms of O_2 reduction in 0.1 M KOH solution at the Pt electrodes that have CA values of (1) 24.0° ± 0.9°, (2) 57.0° ± 0.8°, (3) 82.0° ± 0.5°, and (4) 106.0° ± 0.4°. The scan rate was 50.0 mV s^{-1}.

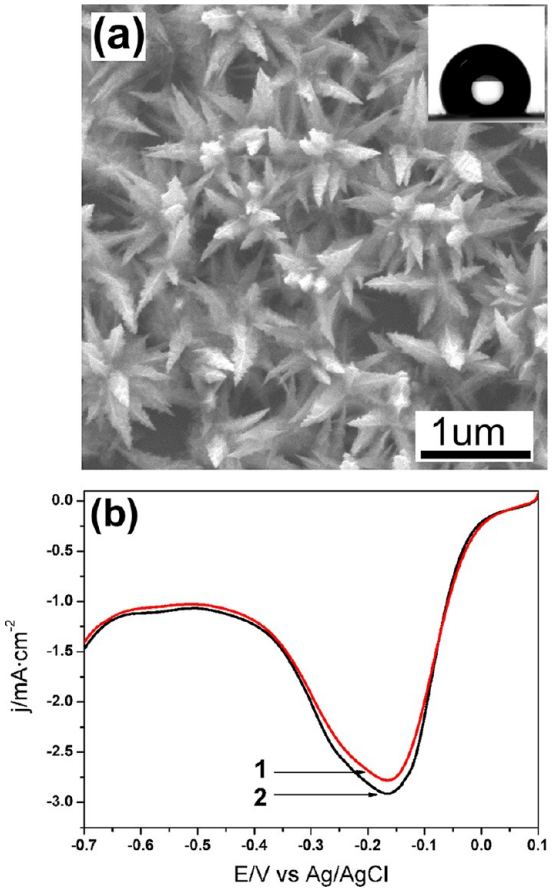

Figure 9. (a) SEM of Pd catalysts having CA = 130° ± 0.3°; (b) linear sweep voltammograms of O_2 in 0.1 M KOH solution at the Pd catalysts that are shown in Figure 1d (curve 1) and panel (a) in this figure (curve 2).

scan of Figure 4b, should originate from the directed oxidation of formate, rather than from the intermediates as speculated. The delay in the emergence of this formate anodic peak may be understood from the small reduction peak in Figure 5, which occurred right before the large anodic peak. Such a reduction peak suggests that Pd(II) ions need to be reduced first in order to catalyze the oxidation of formate. Consequently, their dependence on the surface wettability will be the same as that observed during the forward scan. The above experiments provide a concrete example that the influence of the surface wettability of solid catalysts on their catalytic performance is closely correlated to the physical processes. Analysis of such correlations may lead to new insights into the phase transfer reaction, such as the electrochemical oxidation of formate studied above.

A different type of phase transfer reaction catalyzed by the above Pd catalysts was investigated in Figure 6, which was the reduction of oxygen in alkaline solution. The catalytic reduction of oxygen is a very important process in fuel cells and has attracted a great deal of attention lately.[41,42] As opposed to systems studied in Figure 4, here, the gas molecule is a reactant rather than a product. Linear sweep voltammetry (LSV) of 0.1 M KOH solution saturated with oxygen was presented in Figure 6, where the cathodic peak with the highest current density was achieved at the Pd electrode that had a CA value of 125.0° ± 0.4°, whereas the peak with the lowest magnitude came from the surface with a CA value of 15.0°. In other words, solid catalysts with a hydrophobic surface favor the electrochemical reduction of oxygen. This behavior can be understood based on the fact that a hydrophilic surface offers a tight contact with the electrolyte solution and, thus, reduces the adsorption of oxygen molecules (O_2), which consequently makes the reduction of O_2 more difficult. This series of experiments further confirm that wettability and the nature of a reaction process are intermingled to determine the catalytic performance of solid catalysts. Controlled experiments with systems that do not involve phase transitions (e.g., the redox reaction of 5.0 mM $K_3Fe(CN)_6$ in 0.1 M KCl solution) demonstrate that the surface wettability of Pd catalysts has no effect on their electrochemical behavior. Therefore, besides its importance in developing more efficient catalysts, the correlation between surface wettability and catalytic efficiency could also be employed as a unique tool to gain insights into the mechanisms of multiphase reactions.

To test the generality of the above observation, Pt catalysts with a wide range of surface wettability were also fabricated in this research through the electrochemical approach. Similar to the Pd catalysts, variation in the surface roughness was readily obtained by controlling the deposition time. SEM images in

Figure 7 show the surface morphology of the Pt catalysts prepared with the deposition time of 200 s (Figure 7a), 250 s (Figure 7b), 300 s (Figure 7c), and 350 s (Figure 7d). The analysis indicates that the ITO film was fully covered by platinum particles after 200 s. The phenomenon that the ITO substrate is only partially covered by platinum particles is deceiving, which is due to the effects of large particles on the SEM measurement. The CA values presented in those insets vary from 24.0° to 106.0° ((a) 24.0° ± 0.9°, (b) 57.0° ± 0.8°, (c) 82.0° ± 0.5°, and (d) 106.0° ± 0.4°).

EDX spectra of the above Pt catalysts indicate that those platinum particles are pure. When these Pt catalysts were applied to electro-oxidize H_2O_2, the cyclic voltammograms obtained in Figure 8a were qualitatively the same as those obtained with Pd catalysts (i.e., the catalyst layer with the highest surface wettability produced the largest current density). The observation that the hydrophilic Pt catalysts favor the oxidation is because such a surface provides more available sites for H_2O_2 adsorption through facilitating the escape of gas products. The cyclic voltammograms of the reduction of oxygen in alkaline solution shown in Figure 8b illustrate that the platinum layer with the lowest surface wettability generates the strongest current density, which is also consistent with the behavior of Pd catalysts.

Pd catalysts shown in Figure 1 are composed of particles having similar morphology, but different sizes. The variation in the surface roughness (i.e., surface wettability) is caused by changes of the particle size. We have also attempted to examine Pd catalysts having the same wettability, but different surface morphologies. Figure 9a shows is a layer of Pd catalysts consisting of feather-like particles. CA measurement shows that this surface has a CA value of 130°, which is very close to the catalysts prepared in Figure 1d. When both Pd catalyst layers were applied to catalyze the electro-reduction of oxygen, Figure 9b shows that very similar linear sweep voltammograms were obtained. This result demonstrates that the microstructure of Pd catalysts also affect their chemical activity. In terms of differences in the magnitude of the observed current density, the transformation from hydrophilic to hydrophobic surface seems to insert stronger impacts on the catalysis.

4. CONCLUSIONS

This research presents a convenient approach to fabricate Pd and Pt catalysts with a wide range of surface wettability. No surfactant is required in this electrochemical method. The control on the macroscopic properties of the Pd and Pt catalyst layers led to very different performances in the electro-oxidation of hydrogen peroxide and sodium formate or the reduction of oxygen in alkaline solutions. The above information shall be useful in engineering more efficient cathode and anode catalytic layers for fuel cells. Collectively, this study demonstrates that wettability does not only have important influences on the performance of a solid catalyst, but also can be employed as a beacon to decipher the multiphase reaction mechanisms. Although phase transfer reactions examined in this research all involve gas species, the same outcome on the correlation between wettability and catalytic performance is expected to exist in other forms of multiphase reactions, such as those being carried out in a biphasic mixture of two immiscible solvents.

AUTHOR INFORMATION

Corresponding Author

*Fax: 86-577-86683000 (S.W.), 1-519-973-7098 (J.W.). E-mail: shunwang@wzu.edu.cn (S.W.), jwang@uwindsor.ca (J.W.).

Notes

The authors declare no competing financial interest.

ACKNOWLEDGMENTS

We are grateful for the financial support from NSFC (Nos. 21073133 and 51272182), Zhejiang Provincial Natural Science Foundation of China (Nos. Y4080177, Y4090248, and Y5100283), and the Zhejiang Scientific and Technological Innovation Fund (Nos. 2012R424062 and 2012R424064).

REFERENCES

(1) Guo, S.; Wang, E. *NanoToday* **2011**, *6*, 240−264.
(2) Shao, F.; Sun, J.; Gao, L.; Yang, S.; Luo, J. *ACS Appl. Mater. Interfaces* **2011**, *3*, 2148−2153.
(3) Nesselberger, M.; Ashton, S.; Meier, J. C.; Katsounaros, I.; Mayrhofer, K. J. J.; Arenz, M. *J. Am. Chem. Soc.* **2011**, *133*, 17428−17433.
(4) Chen, W.; Chen, S. *Angew. Chem., Int. Ed.* **2009**, *48*, 4386−4389.
(5) Shao, M.; Peles, A.; Shoemaker, K. *Nano Lett.* **2011**, *11*, 3714−3719.
(6) Sau, T. K.; Rogach, A. L. *Adv. Mater.* **2010**, *22*, 1781−1804.
(7) Fu, W.; Zhang, L.; Tang, T.; Ke, Q.; Wang, S.; Hu, J.; Fang, G.; Li, J.; Xiao, F. S. *J. Am. Chem. Soc.* **2011**, *133*, 15346−15349.
(8) Mazumder, V.; Lee, Y.; Sun, S. *Adv. Funct. Matter.* **2010**, *20*, 1224−1231.
(9) Meng, H.; Xie, F.; Chen, J.; Shen, P. K. *J. Mater. Chem.* **2011**, *21*, 11352−11358.
(10) Ge, J.; Xing, W.; Xue, X.; Liu, C.; Lu, T.; Liao, J. *J. Phys. Chem. C* **2007**, *111*, 17305−17310.
(11) Wang, L.; Nemoto, Y.; Yamauchi, Y. *J. Am. Chem. Soc.* **2011**, *133*, 9674−9677.
(12) Xiao, L.; Zhuang, L.; Liu, Y.; Lu, J.; Abruna, H. D. *J. Am. Chem. Soc.* **2009**, *131*, 602−608.
(13) Huang, X.; Zhao, Z.; Fan, J.; Tan, Y.; Zheng, N. *J. Am. Chem. Soc.* **2011**, *133*, 4718−4721.
(14) Ming, T.; Feng, W.; Tang, Q.; Wang, F.; Sun, L.; Wang, J.; Yan, C. *J. Am. Chem. Soc.* **2009**, *131*, 16350−16351.
(15) Zhou, Z. Y.; Huang, Z. Z.; Chen, D. J.; Wang, Q.; Tian, N.; Sun, S. G. *Angew. Chem., Int. Ed.* **2010**, *49*, 411−414.
(16) Tian, N.; Zhou, Z. Y.; Yu, N. F.; Wang, L. Y.; Sun, S. G. *J. Am. Chem. Soc.* **2010**, *132*, 7580−7581.
(17) Zhang, H.; Jin, M.; Xia, Y. *Angew. Chem., Int. Ed.* **2012**, *51*, 7656−7673.
(18) Suo, Y.; Zhuang, L.; Lu, J. *Angew. Chem., Int. Ed.* **2007**, *46*, 2862−2864.
(19) Wang, C.; Chi, M.; Li, D.; Strmcnik, D.; Vliet, D.; Wang, G.; Komanicky, V.; Chang, K.; Paulikas, A. P.; Tripkovic, D.; Pearson, J.; More, K. L.; Markovic, N. M.; Stamenkovic, V. R. *J. Am. Chem. Soc.* **2011**, *133*, 14396−14403.
(20) Hong, J. W.; Kim, D.; Lee, Y. W.; Kim, M.; Kang, S. W.; Han, S. W. *Angew. Chem., Int. Ed.* **2011**, *123*, 9038−9042.
(21) Zhou, W. P.; Yang, X.; Vukmirovic, M. B.; Koel, B. E.; Jiao, J.; Peng, G.; Mavrikakis, M.; Adzic, R. R. *J. Am. Chem. Soc.* **2009**, *131*, 12755−12762.
(22) Zhang, J.; Vukmirovic, M. B.; Xu, Y.; Mavrikakis, M.; Adzic, R. R. *Angew. Chem., Int. Ed.* **2005**, *44*, 2132−2135.
(23) Vinayan, B. P.; Nagar, R.; Rajalakshmi, N.; Ramaprabhu, S. *Adv. Funct. Mater.* **2012**, *22*, 3519−3526.
(24) Haan, J. L.; Stafford, K. M.; Masel, R. I. *J. Phys. Chem. C* **2010**, *114*, 11665−11672.
(25) Ding, S.; Yin, X.; Lu, X.; Wang, Y.; Huang, F.; Wan, D. *ACS Appl. Mater. Interfaces* **2012**, *4*, 306−311.

(26) Jiang, L.; Zhao, Y.; Zhai, J. *Angew. Chem., Int. Ed.* **2004**, *116*, 4438−4441.
(27) Zhong, Z.; Zhong, Y.; Liu, C.; Yin, S.; Zhang, W.; Shi, D. *Phys. Status Solidi* **2003**, *198*, 197−203.
(28) Yu, H. M.; Ziegler, C.; Oszcipok, M.; Zobel, M.; Hebling, C. *Electrochim. Acta* **2006**, *51*, 1199−1207.
(29) Aguado, S.; Canivet, J.; Schuurman, Y.; Farrusseng, D. *J. Catal.* **2011**, *284*, 207−214.
(30) McVicker, G. B.; Kim, C. J.; Eggert, J. J. *J. Catal.* **1983**, *80*, 315−327.
(31) Wang, Q.; Eikerling, M.; Song, D.; Liu, Z. *J. Electroanal. Chem.* **2004**, *573*, 61−69.
(32) Weber, A. Z.; Darling, R. M.; Newman, J. *J. Electrochem. Soc.* **2004**, *151*, A1715−A1727.
(33) Mies, M. J. M.; Rebrov, E. V.; Jansen, J. C.; de Croon, M. H. J. M.; Schouten, J. C. *J. Catal.* **2007**, *247*, 328−338.
(34) Bianchini, C.; Shen, P. K. *Chem. Rev.* **2009**, *109*, 4183−4206.
(35) Lvovich, V.; Scheeline, A. *Anal. Chem.* **1997**, *69*, 454−462.
(36) Gorton, L. *Anal. Chim. Acta* **1985**, *178*, 247−253.
(37) Hall, S. B.; Khudaish, E. A.; Hart, A. L. *Electrochimim. Acta* **1998**, *43*, 579−588.
(38) Wang, J. Y.; Zhang, H. X.; Jiang, K.; Cai, W. B. *J. Am. Chem. Soc.* **2011**, *133*, 14876−14879.
(39) Jiang, J.; Wieckowski, A. *Electrochem. Commun.* **2012**, *20*, 121−123.
(40) Lim, B.; Jiang, M.; Camargo, P. H. C.; Cho, E. C.; Tao, J.; Lu, X.; Zhu, Y.; Xia, Y. *Science* **2009**, *324*, 1302−1305.
(41) Zhang, C.; Fan, F, R, F.; Bard, A, J. *J. Am. Chem. Soc.* **2009**, *131*, 177−181.
(42) Patra, S.; Viswanath, B.; Barai, K.; Ravishankar, N.; Munichandraiah, N. *ACS Appl. Mater. Interfaces* **2010**, *2*, 2965−2969.

NOTE ADDED AFTER ASAP PUBLICATION

This paper was published on the Web on April 23, 2013, with errors in Figure 9. The corrected version was reposted on April 24, 2013.